Effect of the load direction on non-nominal five-pad tilting-pad journal bearings

Phuoc Vinh Dang[a,b,*], Steven Chatterton[a], Paolo Pennacchi[a], Andrea Vania[a]

[a] Department of Mechanical Engineering, Politecnico di Milano, Via La Masa 1, I-20156 Milan, Italy

[b] Department of Mechanical Engineering, University of Science and Technology - The University of Danang, Nguyen Luong Bang Street, Danang, Viet Nam

Abstract

In this paper, a theoretical analysis of the influence of the load direction on the characteristics of a five-pad tilting-pad journal bearing (TPJB) is investigated. An analysis is performed for a TPJB using a non-nominal geometry, that is, with a different preload factor for each pad. The analytical results are then compared with the experimental measurements for a real bearing having pads with different geometries due to manufacturing errors. The results show that the load direction has considerable effects on both the static and dynamic characteristics of the TPJB. A robust estimation method is introduced for the calculation of experimental dynamic coefficients. The procedure for the bearing geometry estimation from the experimental measurement of the clearance profile is also described.

Keywords: Load directions; non-nominal bearings; tilting-pad journal bearing; five pads.

[*] Corresponding author: Tel. +39 02 23998442

Email address: phuocvinh.dang@polimi.it; dpvinh@dut.udn.vn

Nomenclature

b_G	position of the barycenter with respect to the pivot point in the tangential direction (m)
c_G	position of the barycenter with respect to the pivot point in the radial direction (m)
$[\mathbf{C}]$	linearized damping coefficient matrix
$\left[C_{pad}\right]^k$	Pad damping matrix
$c_{xx},\ c_{xy}, c_{yx}, c_{yy}$	linearized damping coefficients in absolute reference system (Ns/m)
$c_{\xi\xi},\ c_{\xi\zeta}, c_{\zeta\xi}, c_{\zeta\zeta}$	linearized damping coefficients in load reference system (Ns/m)
D	Bearing diameter (m)
E	Young's modulus of pivot and pivot housing (Pa)
J_P	mass moment of inertia of the pad with respect to pivot point (kg.m^2)
F_1, F_2	forces of the two hydraulic actuators (N)
$\Delta F_{x,oil}, \Delta F_{y,oil}$	horizontal and vertical oil-film forces in the frequency domain (N)
$f_{x,oil},\ f_{y,oil}$	horizontal and vertical oil-film forces in the time domain (N) along x and y directions
$f^k_{\theta,oil}, f^k_{\eta,oil}$	moment of the oil-film forces with respect to the pivot and the resultant of the oil-film forces along the radial direction of the pivot position in the time domain (N)
h	oil-film thickness (m)
$\left[K_{pad}\right]^k$	Pad stiffness matrix
$[\mathbf{K}]$	linearized stiffness coefficient matrix
$k_{xx},\ k_{xy}, k_{yx}, k_{yy}$	linearized stiffness coefficients in the absolute reference system (N/m)
$k_{\xi\xi},\ k_{\xi\zeta}, k_{\zeta\xi}, k_{\zeta\zeta}$	linearized damping coefficients in the load reference system (N/m)
$M_{xx},\ M_{xy}, M_{yx}, M_{yy}$	linearized add-mass coefficients (kg)
$c_b,\ c_p$	assembled clearance, machined clearance (m)
$\left[M_{pad}\right]^k$	pad mass matrix

m	pad mass (kg)
m_p	preload factor
L	pad width (m)
p	oil-film pressure (Pa)
r_{pe}	outer radius of the pad (m)
r_{pi}	inner radius of the pad (m)
r_j	journal radius (m)
r_H	bearing housing radius (m)
t	pad thickness (m)
x, y	shaft-to-bearing housing relative displacements in the horizontal and vertical directions in the time domain (m)
$\dot{x}$, $\dot{y}$	shaft-to-bearing housing relative velocity in the horizontal and vertical directions in the time domain (m/s)
$\ddot{x}$, $\ddot{y}$	shaft-to-bearing housing relative acceleration in the horizontal and vertical directions in the time domain (m/s^2)
X,Y	shaft-to-bearing housing relative displacements in the horizontal and vertical directions in the frequency domain (m)
$\dot{X}$,$\dot{Y}$	shaft-to-bearing housing relative velocity in the horizontal and vertical directions in the frequency domain (m)
ε	eccentricity of the journal center (m)
α_k	angle from the *X-axis* to the O_bP about the axial direction of the k^{th} pad (rad)
β_k	pivoted pad angle from the k^{th} pad pivot point to an arbitrary point in the oil bearing (rad)
δ_k	angle from the *X-axis* to the *PK* about the axial direction of the k^{th} pad (rad)
μ	dynamic viscosity of the oil (Pa s)
ρ	mass density of the oil (kg/m^3)
α_v	coefficient of thermal expansion of the oil °C^{-1}
κ	viscosity index of the oil (-)

Ω	journal rotational speed (rad/s)
ω	excitation circular frequency (rad/s)
θ	pad tilt angle (rad)
η	pad radial displacement (m)
ν	Poisson coefficient (-)
Im	imaginary part
Re	real part

1. Introduction

Tilting pad journal bearings (TPJBs) are widely used in high rotating speed machines mainly due to their high stability compared with plain or fixed-arc journal bearings. Because the dynamic behavior of a rotating machine is strongly influenced by the dynamic characteristics of the bearings, TPJBs have been studied extensively by many authors using numerical simulations and experimental tests. In 1964, Lund [1] introduced his "Lund's pad assembly method" consisting of calculating the stiffness and damping coefficients for a single fixed non-rotational pad and then summing the contributions from each pad to find the combined effect of the pad assembly. Lund's design curves did not take into account the radial frequency dependency, and for many years, the common assumption was that the dynamic coefficients should be calculated at the synchronous frequency. Over the years, many effective methods have been applied, such as the Newton-Raphson method, numerical analyses, finite elements methods, and genetic algorithms, to calculate the static and dynamic characteristics of journal bearings [2]-[4].

Strzelecki [5] studied the dynamic characteristics of a five-pad tilting-pad bearing with an asymmetric pad support using the Reynolds equation and an adiabatic model for the oil film. The results showed that the pad clearance influences the stiffness and damping coefficients, whereas the length to diameter ratio just affects the direct stiffness coefficients. The effect of pad compliance on the nonlinear dynamic characteristics of TPJBs was also investigated in [6].

Most of the studies of TPJB in the literature consider load-on-pad (LOP) or load-between-pad (LBP) configurations [7]-[12]. Conversely, studies on the effects of loading direction on the TPJBs are still rare, and most of the papers are limited to theoretical analyses. In 2002, Solghar et al. in [13] experimentally investigated the influence of the loading direction on the thermo-hydrodynamic behavior of a twin axial-groove journal bearing. They observed that the variation in the load direction has a strong effect on the bearing performance. Simmons et al. in [14] investigated the

effect of the load direction on the performances of a 200 mm diameter TPJB. In particular, they concluded that the load direction had a substantial effect on the maximum pad temperature. Furthermore, they showed that large reductions in the oil flow rate were possible, leading to useful energy savings without compromising the reliability of the bearing.

Yin et al. in [15] analyzed the influence of the load directions on the static and dynamic characteristics of tilting pad bearings. The results showed that the load direction has a strong impact on the static and dynamic characteristics of the tilting pad bearing, especially the oil-film force, oil-film thickness, stiffness and damping coefficients. This means that, for operating conditions in which the load direction changes rapidly, studying the LOP and LBP configurations is not sufficient, especially when analysis of the dynamic performances of the tilting pad bearing is needed.

Actually, high bearing loads not in the vertical direction may occur in industrial rotating machines, such as in turbo-generators, due to misalignment conditions of the shaft line [16], or in gearboxes. Jones et al. in [17] studied the theoretical effects of load direction on the steady-state and dynamic behavior of tilting pad journal bearings. These authors concluded that a non-symmetrical direction of the load with respect to the pivot positions can produce significant cross-coupling dynamic terms. Additionally, it was found that changing the direction from LOP to LBP tends to reduce the maximum temperature in the bearing, especially when subject to high loads, with negligible effect on power loss.

Moreover, most of the papers in the literature evaluate the static and dynamic characteristics of TPJBs by means of thermo-hydrodynamic (THD) models but assume nominal dimensions for all bearing pads; that is, the pads have the same nominal geometry, which corresponds to a circular periodicity of the bearing geometry. In real applications, the manufacturing tolerances for the pads can be of the same order of magnitude as the oil-film thickness. Therefore, an actual non-nominal geometry can occur, leading to a mistuned bearing. The main effect is a different preload for each

pad, and the real bearing behavior differs from the behavior calculated using a numerical model. This phenomenon is critical for high-speed shafts with a small diameter, where the necessity for large dynamic coefficients is obtained using small bearing clearances. In the industrial field, the final geometry of the pads is generally adjusted using calibrated shims under the pivots that are able to compensate for the manufacturing tolerances. This solution is not applicable to rocker-backed TPJBs. In real applications, a "mistuned" bearing is difficult to identify during the commissioning phase of the machine. A large difference in the pad temperature can be an indicator of an incorrect preload but also an indicator of shaft misalignment. Furthermore, in the industrial field, only the loaded pads, i.e., the pads along the direction of the load, are equipped with temperature probes (one in case of LOP, two in case of LBP).

Fillon in [18] and [19] investigated using simulations the effect of manufacturing tolerances on the static and dynamic characteristics of a 5-pad TPJB using the same geometry for all pads.

In this paper, the authors investigated the performances a five-pad TPJB under three main conditions, namely: (i) the bearing with real dimensions, i.e., different clearances for each pad; (ii) effect of load direction, i.e., the load direction does not follow the more commonly studied LOP and LBP configuration; and (iii) the experimental measurements have been carried out and compared to numerical simulations.

In this paper the experimental behavior of the bearing due to the loading direction and the non-nominal geometry of the pads is shown first. The test rig and the experimental procedure for the evaluation of the clearance profile and the dynamic coefficients is also described. Then, the unexpected behavior of the bearing is compared to the numerical results of a thermo-hydrodynamic model. Moreover, a robust estimation technique is used for the first time to the best of the author's knowledge for the calculation of the dynamic coefficients. This property has a very precise definition in statistics, as reported in [20]-[22], which is rather impractical to report in detail. To

make the concept easier, the robustness can be assumed to be the insensitivity to data noise and corruption.

2. Description of the bearing under test

The bearing under test, shown in Fig. 1, is a five shoe rocker-backed TPJB. The bearing is installed in its housing in a standard LOP configuration with a nominal diameter of 100 mm and a length–to–diameter ratio of 0.7. All the geometric characteristics of the nominal bearing and the testing conditions are listed in Table 1. All pads are also equipped with temperature and pressure probes [24].

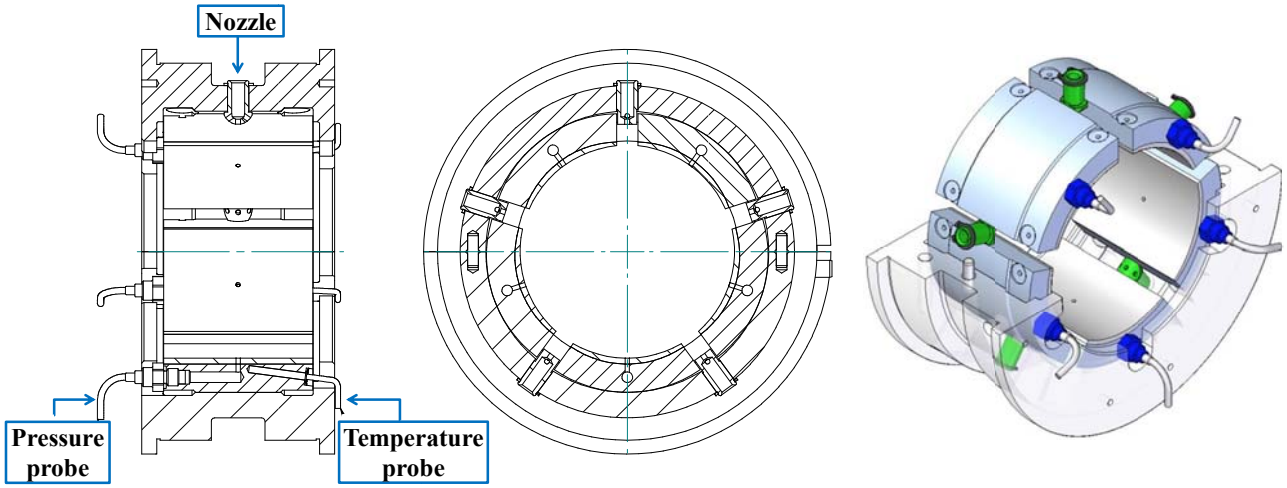

Fig. 1. Five-pad TPJB under test

Table 1. Bearing geometric characteristics and operating conditions

Item	Symbol	Unit	Value/Span
Number of pads			5
Configuration w.r.t bearing housing			LOP
Shaft diameter	$D=2r_j$	mm	100
Bearing length	L	mm	70
Housing radius	r_H	mm	66
Pad outer radius	r_{pe}	mm	59.6
Nominal machined clearance	c_p	mm	0.125
Nominal assembled clearance	c_b	mm	0.070
Preload factor	m_p		0.44
Pad thickness (nominal)	t	mm	16
Angular amplitude of pads		degree (°)	60
Lubricant			ISO VG46
Oil inlet temperature		°C	38-40
Rotational speed		rpm	1200
Static load (on each bearing)		kN	5
Pad mass	m	kg	0.540
Pad mass moment of inertia w.r.t pivot	J_P	kg m^2	0.256E-3

3. Description of the test-rig

The main characteristic of the test rig from the Dept. of Mechanical Engineering of Politecnico di Milano, which is shown in Fig. 2, consists of the supports and the bearing housings.

In the test rig, the rotor axis can describe orbits similar to the real configuration of a rotating machine in which two identical five-pad TPJBs (in the condition of nominal dimensions) which are labeled as **1** and **2** in Fig. 3 support the shaft. Only the bearing #1 which is placed at the non-driven end (**1** in Fig. 3) of the shaft is evaluated for static and dynamic behaviors. The rotor is driven using a 6.0 kW inverter-driven asynchronous electric motor by means of a flexible coupling up to the maximum rotational speed of 3000 rpm. The load is applied in the middle of the shaft by means of two hydraulic actuators arranged in an orthogonal configuration at ±45° with respect to the load cells. The actuators are connected to the shaft by means of two deep-groove high-precision ball

bearings. Due to this configuration, a static load, as well as a dynamic load, can be applied in any direction. The hydraulic actuators have a nominal force of 25 kN, are able to displace the shaft with an amplitude of 100 μm in the frequency band of 0-50 Hz and are provided by the high-resolution position and force transducers. To measure shaft-to-bearing housing relative displacements, two orthogonal proximity probes (**X1A** and **X1B** in Fig. 3) were installed on each bearing support. An additional proximity probe was installed as a keyphasor, which was used for the phase reference of the rotor with respect to the stationary part (housing support) and for the rotor speed measurement. Two accelerometers were placed on the bearing case along the vertical and horizontal directions to account for the inertial forces in the evaluation of the dynamic coefficients. A detailed description of the test rig is given in [24].

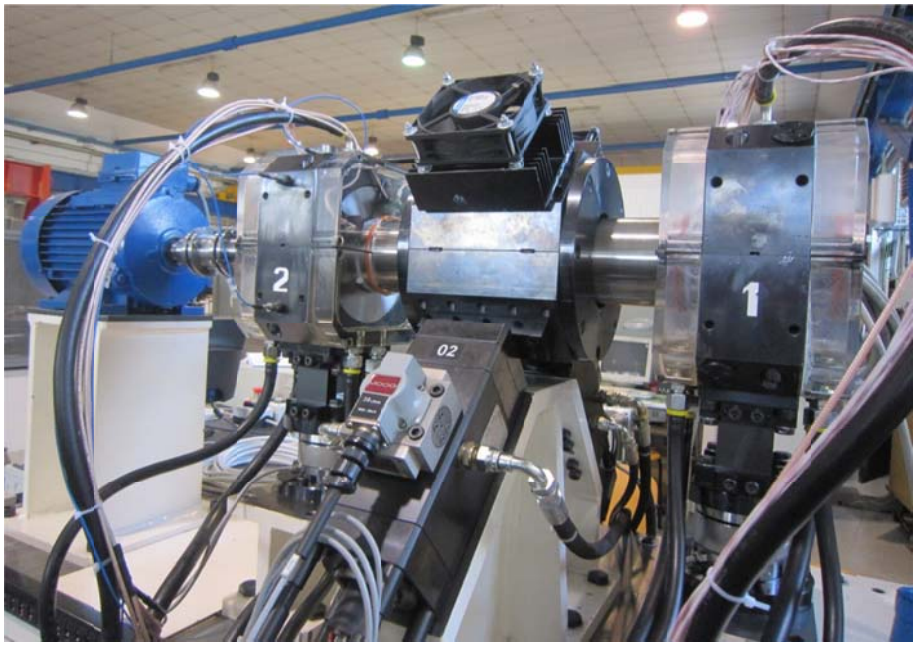

Fig. 2. Picture of the test rig

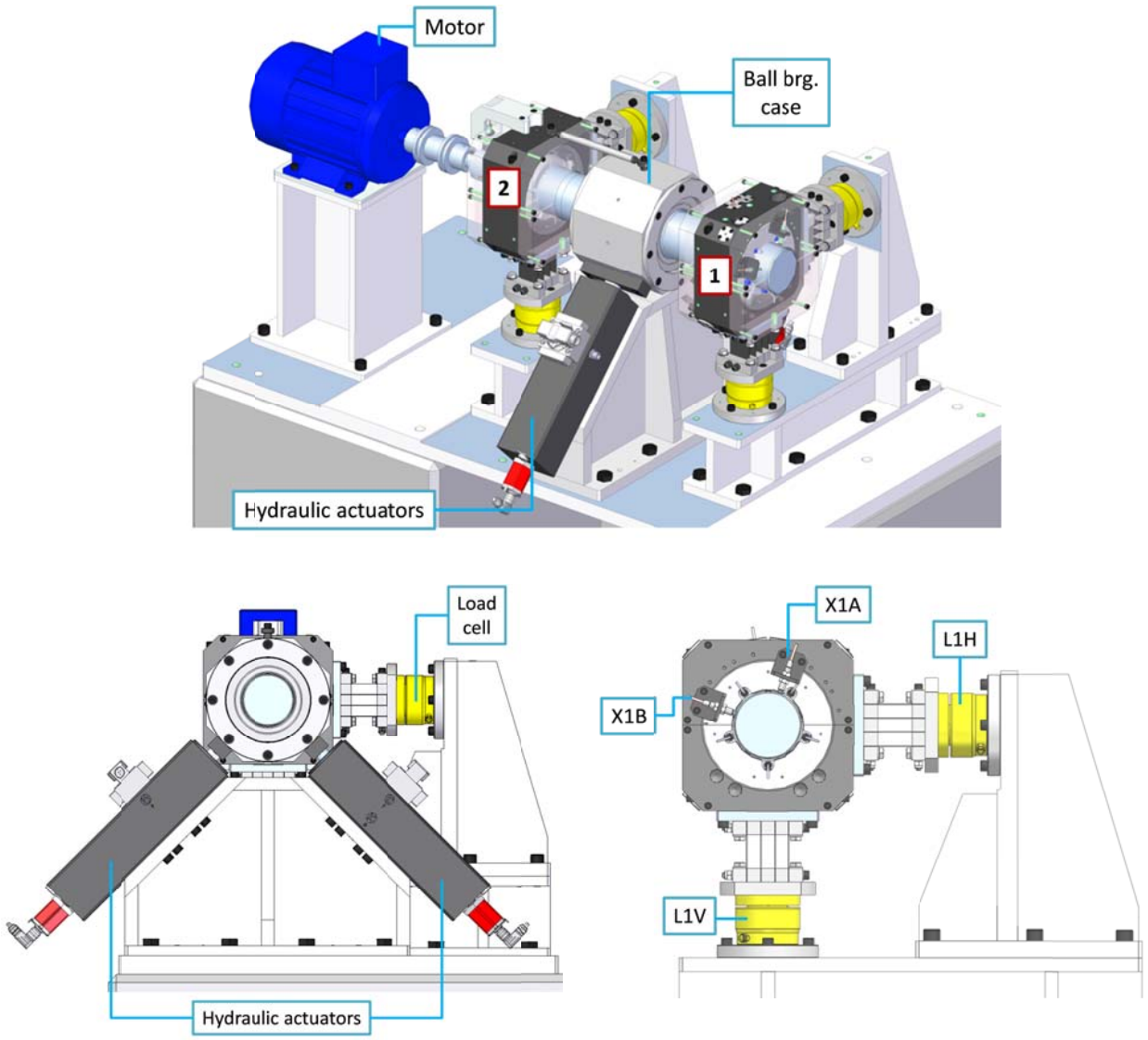

Fig. 3. Test apparatus used for the identification of the bearing behavior

4. Experimental procedure for the evaluation of the dynamic coefficients

The experimental procedure used to evaluate the dynamic coefficients in different loading directions is described in detail in [25],[26],[27] and is shortly summarized hereafter. The direction of the static was varied from −90° (corresponding to the vertical direction, see Fig. 4) to 270° at a step of 18°. In this way, the effect of the non-nominal geometry and the load direction different from the usual LOP and LBP configuration can be tested.

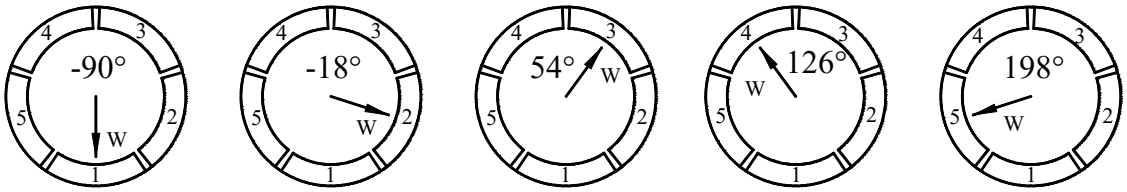

Fig. 4. Varying load configurations

By using the proximity probes, the accelerometers and the load cells installed in the measuring plane corresponding to the NDE bearing, the relative position of the journal with respect to the bearing, the dynamic loads and the absolute acceleration of the bearing housing were measured. A dynamic load of about 10% of the static value has been applied in order to have a dynamic displacement of the shaft with a good signal to noise ratio but not so higher in order to avoid non-linear effects of the oil-film forces. The amplitude of vibration of the shaft was equal to about $2-3\mu m$. To calculate the stiffness and damping coefficients for a given static load, once the journal had reached the equilibrium position (x_0, y_0), the dynamic loads were applied along several different directions to move the shaft in a neighborhood of the equilibrium position, as shown in Fig. 5. In this way, the average behavior of the bearing around the equilibrium position was considered.

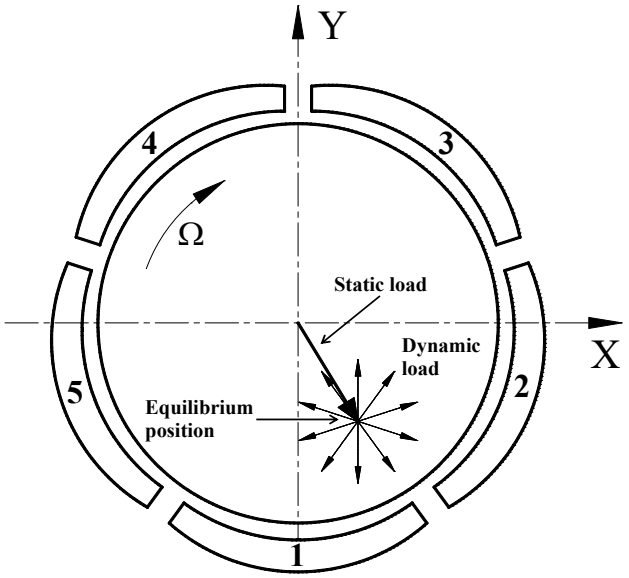

Fig. 5. Static and dynamic loads applied to the shaft for the evaluation of the dynamic coefficients

For the z-th direction of the dynamic excitation, the relationship between the oil-film forces, $\Delta F_{x,oil}(\omega)$ and $\Delta F_{y,oil}(\omega)$ and the amplitudes of vibration, $\Delta X(\omega)$ and $\Delta Y(\omega)$, can be written by applying the harmonic balance in the frequency domain:

$$\begin{bmatrix} \Delta F_{x,oil}(\omega) \\ \Delta F_{y,oil}(\omega) \end{bmatrix}_z = \begin{bmatrix} h_{xx}(\omega) & h_{xy}(\omega) \\ h_{yx}(\omega) & h_{yy}(\omega) \end{bmatrix}_z \begin{bmatrix} \Delta X(\omega) \\ \Delta Y(\omega) \end{bmatrix}_z \tag{1}$$

where $h_{xy}(\omega) = k_{xy}(\omega) + \mathrm{i}\omega c_{xy}(\omega)$ is the complex dynamic coefficients, $\mathrm{i} = \sqrt{-1}$ is the imaginary unit and ω is the circular frequency of the force excitation.

Equation (1) can be rewritten as

$$\begin{bmatrix} \Delta F_{x,oil}(\omega) \\ \Delta F_{y,oil}(\omega) \end{bmatrix}_z = \begin{bmatrix} \Delta X(\omega) & \Delta Y(\omega) & 0 & 0 \\ 0 & 0 & \Delta X(\omega) & \Delta Y(\omega) \end{bmatrix}_z \begin{bmatrix} h_{xx}(\omega) \\ h_{xy}(\omega) \\ h_{yx}(\omega) \\ h_{yy}(\omega) \end{bmatrix} = \left[R(\omega) \right]_z \begin{bmatrix} h_{xx}(\omega) \\ h_{xy}(\omega) \\ h_{yx}(\omega) \\ h_{yy}(\omega) \end{bmatrix} \tag{2}$$

By considering all N directions of the dynamic load, eq. (2) becomes

$$\mathbf{F} = \begin{bmatrix} \left[F\ (\omega)\right]_1 \\ \vdots \\ \left[F\ (\omega)\right]_z \\ \vdots \\ \left[F\ (\omega)\right]_N \end{bmatrix} = \begin{bmatrix} \left[R\ (\omega)\right]_1 \\ \vdots \\ \left[R\ (\omega)\right]_z \\ \vdots \\ \left[R\ (\omega)\right]_N \end{bmatrix} \begin{bmatrix} h_{xx}(\omega) \\ h_{xy}(\omega) \\ h_{yx}(\omega) \\ h_{yy}(\omega) \end{bmatrix} = \left[\mathbf{R}\right]\mathbf{h} \tag{3}$$

The system of equations in (3) is overdetermined, and the vector of the complex dynamic coefficients $\mathbf{h}$ can be obtained by means of a robust M-estimator method ([28],[29]). The M-estimator, introduced by Huber in [22], is based on an *iterated reweighted least squares* (IRLS) algorithm [30], in which, at k-th iteration, the estimate $\hat{\mathbf{h}}$ is given by

$$\hat{\mathbf{h}}^{(k)} = \left(\left[\mathbf{R}\right]^{*\mathrm{T}}\left[\mathbf{W}^{(k-1)}\right]\left[\mathbf{R}\right]\right)^{-1}\left[\mathbf{R}\right]^{*\mathrm{T}}\left[\mathbf{W}^{(k-1)}\right]\mathbf{F} \tag{4}$$

where $\left[\mathbf{W}^{(k-1)}\right] = diag\left(w_i^{(k-1)}\right)$ is the $N \times N$ diagonal matrix of weights.

The weights and estimate are iterated until the values of $\hat{\mathbf{h}}$ converge to a stated criterion. The advantages of robust estimation with respect to a standard least square method is typically explained in the literature ([20],[21]) as having an "automatic" capability to reject data outliers that can influence the estimation of the dynamic coefficients.

Finally, the stiffness and damping coefficients of a system can be evaluated, neglecting the added-mass contribution in the stiffness terms, as:

$$k_{ij} = \mathrm{Re}\left[h_{ij}\right] \tag{5}$$

$$c_{ij} = \frac{\mathrm{Im}\left[h_{ij}\right]}{\omega} \tag{6}$$

All the tests were performed with the shaft rotational speed equal to 1200 rpm (20 Hz) and a static load of 5 kN on each bearing, whereas the frequency of the force excitation ω was equal to 22 Hz. In this way, a quasi-synchronous excitation was assumed. The slight difference between the

shaft frequency and the force frequency was introduced to extract only the contribution of the exciting force from the spectrum of the response and to neglect the effect of the residual unbalance excitation. The exciting frequency is lower than the natural frequencies of the system, therefore no dynamic amplification of the system response, i.e., shaft vibration, occurs in the experimental evaluation of dynamic coefficients. The natural frequencies of the system have been identified by impact tests. The first significant natural frequencies have been identified at 104 Hz and 137 Hz, corresponding to a rotational vibrating mode and a horizontal vibrating mode of the bearing case, respectively. The first bending mode of the rotor has been evaluated with a finite beam element model and is equal to 450 Hz.

5. Estimation of the bearing geometry

The clearance profile is given by the maximum reachable position of the center of the shaft. For a TPJB, the shape of the clearance profile is similar to a polygon having a number of sides corresponding to the number of pads in the bearing [32],[33],[34].

The theoretical clearance profile is a function of the bearing geometry: namely, the thickness (t), pad inner radius (r_{pi}), pad outer radius (r_{pe}), bearing housing radius (r_H) journal radius (r_j) and machined clearance (c_p) of each pad:

$$c_b = f\left(t, r_{pi}, r_{pe,} r_H, r_j, c_p\right) \tag{7}$$

The theoretical clearance profile can be simply obtained by the kinematics of the pad-shaft system. In particular, by considering pad #1 in Fig. 6, points O_k of the clearance profile are obtained by applying an angular rotation to the pad and obtaining the minimum position of the contact point K_k along the vertical direction, which corresponds to the maximum attainable position of the shaft with respect to the center of the bearing. The procedure is then repeated for all the pads, obtaining

the trajectories of the center of the shaft, as shown in Fig. 7, for the nominal dimensions listed in Table 1.

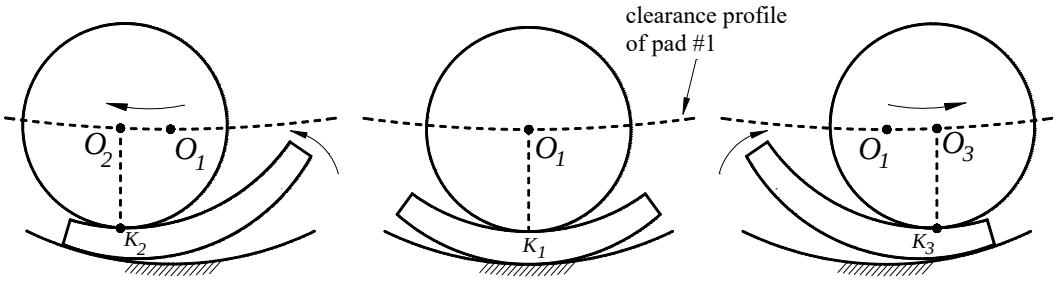

Fig. 6. Method for obtaining the theoretical clearance profile

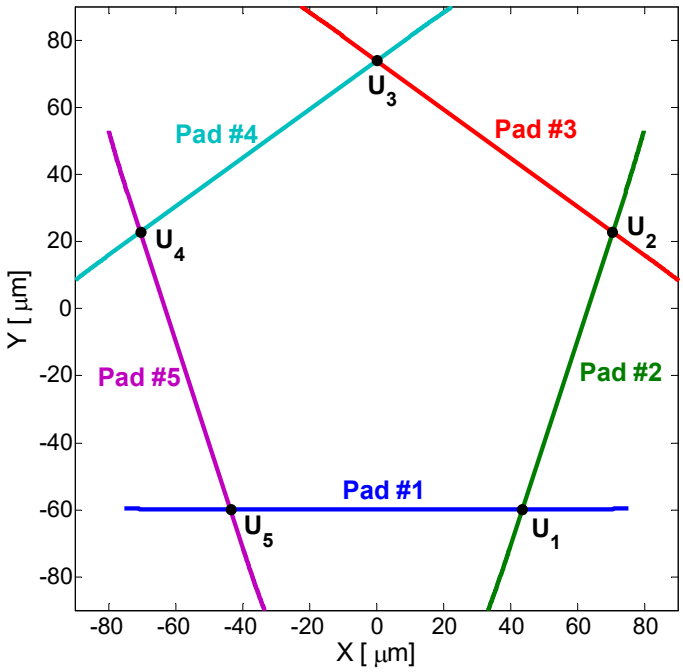

Fig. 7. Trajectories of the shaft center position for the clearance profile

As shown in Fig. 8, the predicted clearance profile of the bearing under test with nominal dimensions (all pads have same dimensions) is similar to a regular pentagon with an average clearance of approximately 60 μm (black dashed-dotted line).

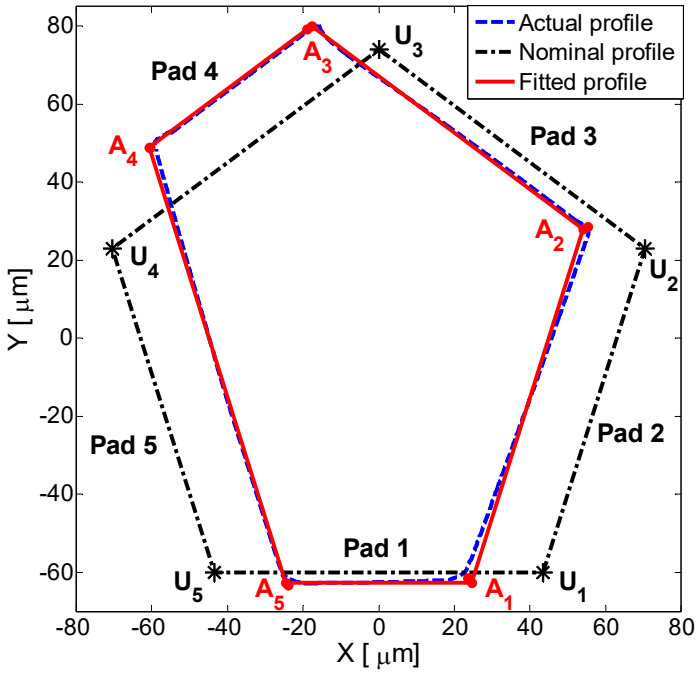

Fig. 8. Actual, nominal, and fitted clearance profile

The actual clearance profile of the bearing under test was measured using the proximity probes installed on the test rig, which are able to measure the relative displacement between the bearing housing and the shaft. The non-rotating rotor was slowly moved inside the housing support by means of a very low-frequency rotating force applied in the middle of the shaft by the two hydraulic actuators [24]. The rotating resultant force was chosen to:

- ensure that each pad is loaded by the exerted thrust along its span;
- be sufficiently high to put the shaft in contact with all the pads;
- to prevent significant pivot deflections during the tests.

The actual clearance profile of the bearing under test (blue dashed line in Fig. 8) is very different from that of the nominal profile, probably due to manufacturing errors of the pads. Taking into account the manufacturing process of the pads, it is likely that the error can be introduced during the

positioning of the pad for the milling process of the internal surface of the pad, which results in a different thickness of the pad at the pivot position.

To predict the behavior of the bearing under test by simulation, an estimation of the actual bearing geometry must first be carried out. In particular, it is assumed that the bearing has the nominal dimensions listed in Table 1 except for the pad thickness, which is different for each pad. The estimation of the pad thickness was performed by fitting the kinematic model of the clearance profile with the actual profile.

In particular, the five points at the vertexes of the pentagon-shaped profile can be identified by interpolation for both the actual (A1 ÷ A5) and theoretical (U1 ÷ U5) profiles, as shown in Fig. 8. The estimation of the bearing geometry can be achieved by minimizing the following objective function:

$$\vartheta = \sqrt{\sum_{k=1}^{N_{pads}} \left[\left(x_{U_k} - x_{A_k} \right)^2 + \left(y_{U_k} - y_{A_k} \right)^2 \right]} \tag{8}$$

The estimated pad thicknesses and the corresponding assembled clearances and preload factors are listed in Table 2.

Table 2. Estimated geometry of the TPJB under test

	Nominal	**Pad #1**	**Pad #2**	**Pad #3**	**Pad #4**	**Pad #5**
Pad thickness t [mm]	16.000	15.994	16.015	15.999	15.981	16.018
Assembled clearance c_b [mm]	0.070	0.066	0.045	0.061	0.078	0.042
Preload factor m_p	0.44	0.47	0.64	0.52	0.37	0.66

It is interesting to note that the clearance profile of the bearing under test appears to shrink for pad #2 and pad #5 and stretch for pad #4. The thicknesses of pad #2 and pad #5 of the bearing under test are greater than the thickness of the nominal bearing by approximately 15 μm and 18 μm,

respectively. For this reason, there is a contraction in the clearance profile for pad #2 and #5. Conversely, pad #4 has the smallest thickness (15.981 mm), so the displacement of the shaft will be largest for pad #4.

6. THD bearing model

The main advantage of a TPJB consists of the pads' capability to follow the displacements of the rotor. During operation, each pad rotates such that the resultant of the fluid-film forces and the inertial forces due to the mass of the pad passes through the pivot or the contact point between the pad and the bearing ring. Therefore, the pivot location influences the pad rotation and the magnitude of the hydrodynamic pressure distribution.

The bearing model includes the effect of the pad inertia and the pivot stiffness [32], the hydrodynamic lubrication model for the pressure distribution and a simple thermal model for the effect of the temperature distribution on the oil viscosity.

Fig. 9 shows in detail the geometry of a single pad from the five shoe rocker-backed TPJB, where O_b and O_j denote the center of the bearing and the journal, respectively.

The pad tilts about the line contact, whose trace is the pivot P. Point P is also able to moves along the radial direction η due to the flexibility of the pivot. The tangential displacement of the point P is neglected. For a given static load, the static equilibrium configuration of the pads (θ_0, η_0) and the corresponding position of the journal center (x_0, y_0) are calculated using a Newton–Raphson method.

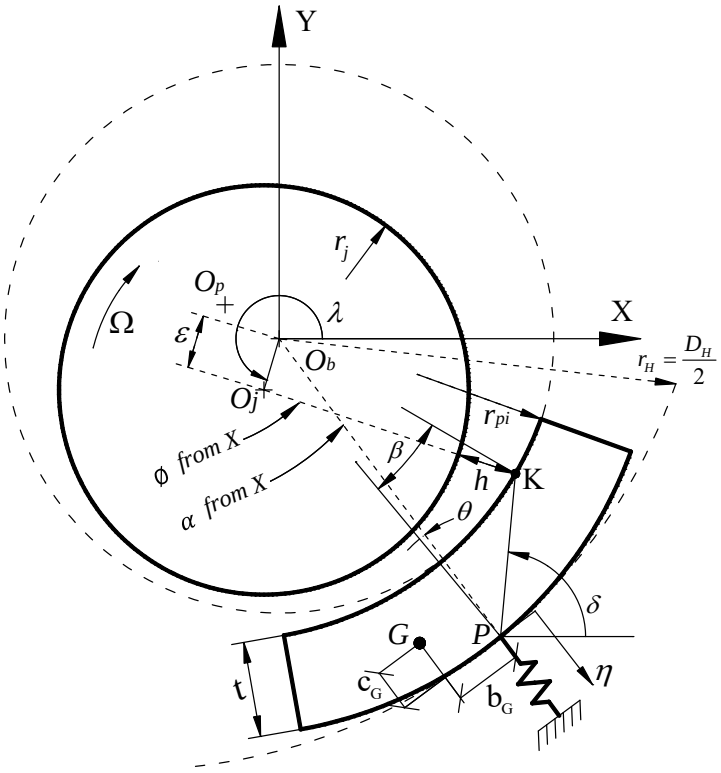

Fig. 9. Geometry and coordinate for a single pad

The first step of modeling the hydrodynamic bearings is the definition of the equation of the oil-film thickness h as a function of the eccentricity and attitude angle, the pad tilt angle and the pad pivoting position.

The pressure distributions of the oil film on each pad are obtained by integrating the Reynolds equation:

$$\frac{\partial}{\partial x}\left(\frac{\rho h^3}{\mu}\frac{\partial p}{\partial x}\right)+\frac{\partial}{\partial z}\left(\frac{\rho h^3}{\mu}\frac{\partial p}{\partial z}\right)=6\left[\left(U_1-U_2\right)\frac{\partial}{\partial x}\left(\rho h\right)+\rho h\frac{\partial}{\partial x}\left(U_1+U_2\right)+2\rho\left(V_2-V_1\right)\right] \tag{9}$$

where h is the oil-film thickness, p is the pressure in the fluid film, μ is the lubricant dynamic viscosity, z is the axial direction, x is the tangential direction, and ρ is the density of the oil. The velocity vector components of the shaft and the pads are described by U_1, V_1 and U_2, V_2, respectively [23].

In particular, the viscosity μ and the density ρ of the lubricating oil are assumed to be functions of only the temperature T :

$$\mu(T) = \mu_{40°C} \exp\left\{\kappa\left(T_{40°C} - T\right)\right\} \tag{10}$$

$$\rho(T) = \rho_{40°C} \exp\left\{1 + \alpha_v\left(T_{40°C} - T\right)\right\} \tag{11}$$

where κ and α_v are the viscosity index and the coefficient of thermal expansion of the oil, respectively. In this research, ISO-VG 46 oil was used for bearing lubrication, and its specifications are listed in Table 3.

Table 3. Specifications of ISO-VG46 lubricant

Viscosity of oil (40°C)	μ	46 Pa.s
Density of oil (40°C)	ρ	861 kg/m^3
Specific heat (40°C)	c_p	1.9766 kJ/(kg/°K)
Coefficient of thermal expansion	α_v	7.34e-4 C^{-1}
Viscosity index of oil	κ	96.552

The oil film forces in the rotor bearing system can be obtained by:

$$\begin{aligned} f_{x,oil} + W_x &= 0 \\ f_{y,oil} + W_y &= 0 \end{aligned} \tag{12}$$

where $f_{x,oil}$ and $f_{y,oil}$ are the horizontal and vertical hydrodynamic oil-film forces acting on the shaft. W_x and W_y are the resultant forces on the shaft due to the shaft inertia and external load along the horizontal and the vertical direction.

By considering a perturbation Δf_{oil} in the oil-film forces with respect to the static value $f_{oil,0}$ at equilibrium:

$$
\begin{aligned}
f_{x,oil} &= f_{x,oil,0} + \Delta f_{x,oil} = \sum_k f^k_{x,oil,0} + \sum_k \Delta f^k_{x,oil} \\
f_{y,oil} &= f_{y,oil,0} + \Delta f_{y,oil} = \sum_k f^k_{y,oil,0} + \sum_k \Delta f^k_{y,oil}
\end{aligned}
\tag{13}
$$

the oil-film forces on the shaft are obtained by the sum of the oil-film forces Δf^k_{oil} of each k-th pad. The forces $\Delta f^k_{oil} = \Delta f^k_{oil}\left(\Delta x, \Delta y, \Delta\theta, \Delta\eta, \Delta\dot{x}, \Delta\dot{y}, \Delta\dot{\theta}, \Delta\dot{\eta}\right)$ on each pad can be linearized about the equilibrium position by means of the full dynamic coefficients:

$$
\begin{aligned}
\Delta f^k_{x,oil} &= -k^k_{xx}\Delta x - k^k_{xy}\Delta y - k^k_{x\theta}\Delta\theta - k^k_{x\eta}\Delta\eta - c^k_{xx}\Delta\dot{x} - c^k_{xy}\Delta\dot{y} - c^k_{x\theta}\Delta\dot{\theta} - c^k_{x\eta}\Delta\dot{\eta} \\
\Delta f^k_{y,oil} &= -k^k_{yx}\Delta x - k^k_{yy}\Delta y - k^k_{y\theta}\Delta\theta - k^k_{y\eta}\Delta\eta - c^k_{yx}\Delta\dot{x} - c^k_{yy}\Delta\dot{y} - c^k_{y\theta}\Delta\dot{\theta} - c^k_{y\eta}\Delta\dot{\eta} \\
\Delta f^k_{\theta,oil} &= -k^k_{\theta x}\Delta x - k^k_{\theta y}\Delta y - k^k_{\theta\theta}\Delta\theta - k^k_{\theta\eta}\Delta\eta - c^k_{\theta x}\Delta\dot{x} - c^k_{\theta y}\Delta\dot{y} - c^k_{\theta\theta}\Delta\dot{\theta} - c^k_{\theta\eta}\Delta\dot{\eta} \\
\Delta f^k_{\eta,oil} &= -k^k_{\eta x}\Delta x - k^k_{\eta y}\Delta y - k^k_{\eta\theta}\Delta\theta - k^k_{\eta\eta}\Delta\eta - c^k_{\eta x}\Delta\dot{x} - c^k_{\eta y}\Delta\dot{y} - c^k_{\eta\theta}\Delta\dot{\theta} - c^k_{\eta\eta}\Delta\dot{\eta}
\end{aligned}
\tag{14}
$$

where θ and η are the angular rotation and the radial displacement of the *k-th* pad respectively, $\Delta f^k_{\theta,oil}$ and $\Delta f^k_{\eta,oil}$ the moment of the oil-film forces with respect to the pivot and the resultant of the oil-film forces along the radial direction of the pivot position.

By considering a harmonic excitation with a forcing frequency ω, the motion of the system will be:

$$
\begin{aligned}
\Delta x(t) &= \Delta X(\omega)e^{\mathrm{i}\omega t} \qquad \Delta\dot{X}(\omega) = \mathrm{i}\,\omega\Delta X(\omega) \\
\Delta y(t) &= \Delta Y(\omega)e^{\mathrm{i}\omega t} \qquad \Delta\dot{Y}(\omega) = \mathrm{i}\,\omega\Delta Y(\omega) \\
\Delta\theta(t) &= \Delta\Theta(\omega)e^{\mathrm{i}\omega t} \qquad \Delta\dot{\Theta}(\omega) = \mathrm{i}\,\omega\Delta\Theta(\omega) \\
\Delta\eta(t) &= \Delta\mathrm{N}(\omega)e^{\mathrm{i}\omega t} \qquad \Delta\dot{\mathrm{N}}(\omega) = \mathrm{i}\,\omega\Delta\mathrm{N}(\omega)
\end{aligned}
\tag{15}
$$

For each pad, the amplitude of oil-film forces in frequency domain can be expressed by:

$$
\begin{bmatrix} \Delta F_{x,oil} \\ \Delta F_{y,oil} \\ \Delta F_{\theta,oil} \\ \Delta F_{\eta,oil} \end{bmatrix}^k
= -\begin{bmatrix} Z_{xx} & Z_{xy} & Z_{x\theta} & Z_{x\eta} \\ Z_{yx} & Z_{yy} & Z_{y\theta} & Z_{y\eta} \\ Z_{\theta x} & Z_{\theta y} & Z_{\theta\theta} & Z_{\theta\eta} \\ Z_{\eta x} & Z_{\eta y} & Z_{\eta\theta} & Z_{\eta\eta} \end{bmatrix}^k
\begin{bmatrix} \Delta X \\ \Delta Y \\ \Delta\Theta_k \\ \Delta\mathrm{N}_k \end{bmatrix}
\tag{16}
$$

where the matrix of the full dynamic coefficients is given by:

$$\begin{bmatrix} Z_{xx} & Z_{xy} & Z_{x\theta} & Z_{x\eta} \\ Z_{yx} & Z_{yy} & Z_{y\theta} & Z_{y\eta} \\ Z_{\theta x} & Z_{\theta y} & Z_{\theta\theta} & Z_{\theta\eta} \\ Z_{\eta x} & Z_{\eta y} & Z_{\eta\theta} & Z_{\eta\eta} \end{bmatrix}^k = \begin{bmatrix} k_{xx} & k_{xy} & k_{x\theta} & k_{x\eta} \\ k_{yx} & k_{yy} & k_{y\theta} & k_{y\eta} \\ k_{\theta x} & k_{\theta y} & k_{\theta\theta} & k_{\theta\eta} \\ k_{\eta x} & k_{\eta y} & k_{\eta\theta} & k_{\eta\eta} \end{bmatrix}^k + \mathrm{i}\omega \begin{bmatrix} c_{xx} & c_{xy} & c_{x\theta} & c_{x\eta} \\ c_{yx} & c_{yy} & c_{y\theta} & c_{y\eta} \\ c_{\theta x} & c_{\theta y} & c_{\theta\theta} & c_{\theta\eta} \\ c_{\eta x} & c_{\eta y} & c_{\eta\theta} & c_{\eta\eta} \end{bmatrix}^k \tag{17}$$

The dynamic coefficients for each pad are obtained using a numerical differentiation approach:

$$[\mathbf{K}]^k = \begin{bmatrix} k_{xx} & k_{xy} & k_{x\theta} & k_{x\eta} \\ k_{yx} & k_{yy} & k_{y\theta} & k_{y\eta} \\ k_{\theta x} & k_{\theta y} & k_{\theta\theta} & k_{\theta\eta} \\ k_{\eta x} & k_{\eta y} & k_{\eta\theta} & k_{\eta\eta} \end{bmatrix}^k = \begin{bmatrix} \left.\frac{\partial f_{x,oil}}{\partial x}\right|_0 & \left.\frac{\partial f_{x,oil}}{\partial y}\right|_0 & \left.\frac{\partial f_{x,oil}}{\partial \theta}\right|_0 & \left.\frac{\partial f_{x,oil}}{\partial \eta}\right|_0 \\ \left.\frac{\partial f_{y,oil}}{\partial x}\right|_0 & \left.\frac{\partial f_{y,oil}}{\partial y}\right|_0 & \left.\frac{\partial f_{y,oil}}{\partial \theta}\right|_0 & \left.\frac{\partial f_{y,oil}}{\partial \eta}\right|_0 \\ \left.\frac{\partial f_{\theta,oil}}{\partial x}\right|_0 & \left.\frac{\partial f_{\theta,oil}}{\partial y}\right|_0 & \left.\frac{\partial f_{\theta,oil}}{\partial \theta}\right|_0 & \left.\frac{\partial f_{\theta,oil}}{\partial \eta}\right|_0 \\ \left.\frac{\partial f_{\eta,oil}}{\partial x}\right|_0 & \left.\frac{\partial f_{\eta,oil}}{\partial y}\right|_0 & \left.\frac{\partial f_{\eta,oil}}{\partial \theta}\right|_0 & \left.\frac{\partial f_{\eta,oil}}{\partial \eta}\right|_0 \end{bmatrix}^k \tag{18}$$

$$[\mathbf{C}]^k = \begin{bmatrix} c_{xx} & c_{xy} & c_{x\theta} & c_{x\eta} \\ c_{yx} & c_{yy} & c_{y\theta} & c_{y\eta} \\ c_{\theta x} & c_{\theta y} & c_{\theta\theta} & c_{\theta\eta} \\ c_{\eta x} & c_{\eta y} & c_{\eta\theta} & c_{\eta\eta} \end{bmatrix}^k = \begin{bmatrix} \left.\frac{\partial f_{x,oil}}{\partial \dot{x}}\right|_0 & \left.\frac{\partial f_{x,oil}}{\partial \dot{y}}\right|_0 & \left.\frac{\partial f_{x,oil}}{\partial \dot{\theta}}\right|_0 & \left.\frac{\partial f_{x,oil}}{\partial \dot{\eta}}\right|_0 \\ \left.\frac{\partial f_{y,oil}}{\partial \dot{x}}\right|_0 & \left.\frac{\partial f_{y,oil}}{\partial \dot{y}}\right|_0 & \left.\frac{\partial f_{y,oil}}{\partial \dot{\theta}}\right|_0 & \left.\frac{\partial f_{y,oil}}{\partial \dot{\eta}}\right|_0 \\ \left.\frac{\partial f_{\theta,oil}}{\partial \dot{x}}\right|_0 & \left.\frac{\partial f_{\theta,oil}}{\partial \dot{y}}\right|_0 & \left.\frac{\partial f_{\theta,oil}}{\partial \dot{\theta}}\right|_0 & \left.\frac{\partial f_{\theta,oil}}{\partial \dot{\eta}}\right|_0 \\ \left.\frac{\partial f_{\eta,oil}}{\partial \dot{x}}\right|_0 & \left.\frac{\partial f_{\eta,oil}}{\partial \dot{y}}\right|_0 & \left.\frac{\partial f_{\eta,oil}}{\partial \dot{\theta}}\right|_0 & \left.\frac{\partial f_{\eta,oil}}{\partial \dot{\eta}}\right|_0 \end{bmatrix}^k \tag{19}$$

where $[\mathbf{K}]^k$ and $[\mathbf{C}]^k$ are the linear stiffness and damping coefficient matrices; $(x_0, y_0, \theta_0, \eta_0, 0, 0, 0, 0)$ represents the static equilibrium position of the system (shaft and pads).

Eq. (16) can be rewritten as:

$$\begin{bmatrix}\Delta F_{x,oil}\\ \Delta F_{y,oil}\end{bmatrix}^k = -\begin{bmatrix}Z_{xx} & Z_{xy}\\ Z_{yx} & Z_{yy}\end{bmatrix}^k\begin{bmatrix}\Delta X\\ \Delta Y\end{bmatrix} - \begin{bmatrix}Z_{x\theta} & Z_{x\eta}\\ Z_{y\theta} & Z_{y\eta}\end{bmatrix}^k\begin{bmatrix}\Delta\Theta\\ \Delta\mathrm{N}\end{bmatrix}^k$$
$$\begin{bmatrix}\Delta F_{\theta,oil}\\ \Delta F_{\eta,oil}\end{bmatrix}^k = -\begin{bmatrix}Z_{\theta x} & Z_{\theta y}\\ Z_{\eta x} & Z_{\eta y}\end{bmatrix}^k\begin{bmatrix}\Delta X\\ \Delta Y\end{bmatrix} - \begin{bmatrix}Z_{\theta\theta} & Z_{\theta\eta}\\ Z_{\eta\theta} & Z_{\eta\eta}\end{bmatrix}^k\begin{bmatrix}\Delta\Theta\\ \Delta\mathrm{N}\end{bmatrix}^k \quad (20)$$

From the equation of motion of each pad, amplitudes of vibration along θ and η are given by:

$$\begin{bmatrix}\Delta\Theta\\ \Delta\mathrm{N}\end{bmatrix}^k = \left(-\omega^2\left[M_{pad}\right]^k + \mathrm{i}\omega\left[C_{pad}\right]^k + \left[K_{pad}\right]^k\right)^{-1}\begin{bmatrix}\Delta F_{\theta,oil}\\ \Delta F_{\eta,oil}\end{bmatrix}^k \quad (21)$$

where $\left[M_{pad}\right]^k$, $\left[C_{pad}\right]^k$ and $\left[K_{pad}\right]^k$ are the mass, the damping and the stiffness matrices of the pad, representing the inertia, the damping and stiffness of the pivot respectively:

$$\left[M_{pad}\right]^k = \begin{bmatrix}J_P & m b_G\\ m b_G & m\end{bmatrix}^k$$
$$\left[C_{pad}\right]^k = \begin{bmatrix}c_\theta & 0\\ 0 & c_\eta\end{bmatrix}^k \quad (22)$$
$$\left[K_{pad}\right]^k = \begin{bmatrix}k_\theta & 0\\ 0 & k_\eta\end{bmatrix}^k$$

where J_P is the mass moment of inertia of the pad with respect to pivot point P, m the mass and b_G the position of the barycenter with respect to the pivot. The parameters c_θ, c_η and k_θ have been neglected and only the pivot stiffness k_η has been considered in the evaluation of the dynamic coefficients.

The stiffness of the pivot along the direction η is obtained by the contact Hertz theory as [35]:

$$k_\eta = \frac{\pi EL}{2\left(1-\nu^2\right)\left[\frac{2}{3} + \ln\frac{8EL\left(r_H - r_{pe}\right)}{2.15^2 F_{P0}}\right]} \quad (23)$$

where E and ν are the Young's modulus and the Poisson coefficient respectively, r_H and r_{pe} are the radii of the bearing housing and pivot and F_{P0} is the load along the radial direction of the pivot. Therefore from eqs. (20) and (21):

$$\begin{bmatrix} \Delta\Theta \\ \Delta\mathrm{N} \end{bmatrix}^k = -\left(\begin{bmatrix} Z_{\theta\theta} & Z_{\theta\eta} \\ Z_{\eta\theta} & Z_{\eta\eta} \end{bmatrix}^k - \omega^2 \left[M_{pad} \right]^k + \mathrm{i}\omega \left[C_{pad} \right]^k + \left[K_{pad} \right]^k \right)^{-1} \begin{bmatrix} Z_{\theta x} & Z_{\theta y} \\ Z_{\eta y} & Z_{\eta y} \end{bmatrix}^k \begin{bmatrix} \Delta X \\ \Delta Y \end{bmatrix} \tag{24}$$

From eq. (13) in the frequency domain, it is possible to obtain the reduced set of dynamic coefficients $[\mathbf{Z}] = [\mathbf{K}] + \mathrm{i}\omega[\mathbf{C}]$:

$$\begin{aligned} &\begin{bmatrix} \Delta F_{x,oil} \\ \Delta F_{y,oil} \end{bmatrix} = -\begin{bmatrix} \sum_k \Delta F_{x,oil}^k \\ \sum_k \Delta F_{y,oil}^k \end{bmatrix} = -\sum_k \left(-\begin{bmatrix} Z_{xx} & Z_{xy} \\ Z_{yx} & Z_{yy} \end{bmatrix}^k \begin{bmatrix} \Delta X \\ \Delta Y \end{bmatrix} - \begin{bmatrix} Z_{x\theta} & Z_{x\eta} \\ Z_{y\theta} & Z_{y\eta} \end{bmatrix}^k \begin{bmatrix} \Delta\Theta \\ \Delta\mathrm{N} \end{bmatrix}^k \right) = \\ &= \sum_k \left(\begin{bmatrix} Z_{xx} & Z_{xy} \\ Z_{yx} & Z_{yy} \end{bmatrix}^k - \begin{bmatrix} Z_{x\theta} & Z_{x\eta} \\ Z_{y\theta} & Z_{y\eta} \end{bmatrix}^k \left(\begin{bmatrix} Z_{\theta\theta} & Z_{\theta\eta} \\ Z_{\eta\theta} & Z_{\eta\eta} \end{bmatrix}^k - \omega^2 \left[M_{pad} \right]^k + \mathrm{i}\omega \left[C_{pad} \right]^k + \left[K_{pad} \right]^k \right)^{-1} \begin{bmatrix} Z_{\theta x} & Z_{\theta y} \\ Z_{\eta y} & Z_{\eta y} \end{bmatrix}^k \right) \begin{bmatrix} \Delta X \\ \Delta Y \end{bmatrix} = \\ &= -\begin{bmatrix} Z_{xx} & Z_{xy} \\ Z_{yx} & Z_{yy} \end{bmatrix} \begin{bmatrix} \Delta X \\ \Delta Y \end{bmatrix} = -[\mathbf{Z}] \begin{bmatrix} \Delta X \\ \Delta Y \end{bmatrix} \end{aligned} \tag{25}$$

In the literature, the dynamic coefficients are evaluated by considering the load acting in the opposite direction of the Y axis (Fig. 10a). If the direction of the load changes, it is still possible to evaluate the dynamic coefficients in the reference system of the load where the Y' axis is aligned in the opposite direction of the load (Fig. 10b) by means of the following transformations:

$$\left[\mathbf{K}' \right] = [\mathbf{R}]^T [\mathbf{K}][\mathbf{R}] \tag{26}$$

$$\left[\mathbf{C}' \right] = [\mathbf{R}]^T [\mathbf{C}][\mathbf{R}] \tag{27}$$

where $[\mathbf{R}]$ is a rotation matrix

$$[\mathbf{R}] = \begin{bmatrix} \cos\beta & -\sin\beta \\ \sin\beta & \cos\beta \end{bmatrix} \tag{28}$$

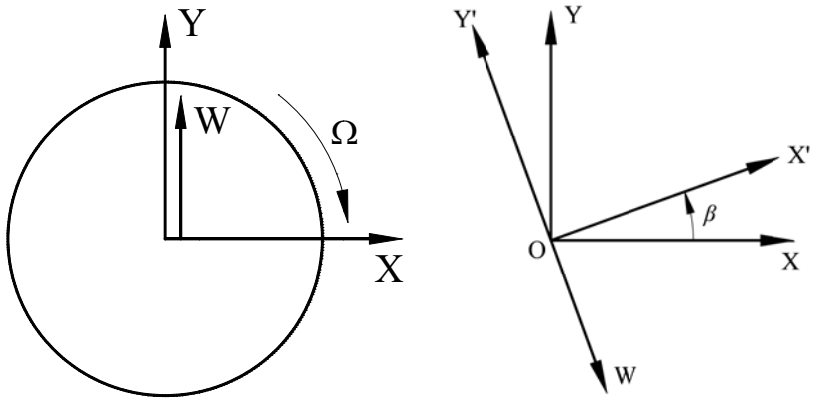

(a) (b)

Fig. 10. Direction of the load with respect to the reference system

A finite-difference code has been developed for the integration of the Reynolds equation. For instance, the pressure $p_{i,j}$ at node (i, j) of the mesh grid is given by a combination of pressures of the nearest nodes:

$$p_{i,j} = a_0 + a_1 p_{i+1,j} + a_2 p_{i-1,j} + a_3 p_{i,j+1} + a_4 p_{i,j-1} \tag{29}$$

A simple two-dimensional control-volume thermal model [36] is considered for the evaluation of the bearing fluid temperatures and viscosities. A constant average temperature of the oil in the radial direction (y) and adiabatic conditions at the pad and shaft surfaces are considered. A more realistic isothermal condition for the shaft can be obtained using a more sophisticated but time-consuming three-dimensional model. For instance, the temperature T_P of the center (**P**ole) of each control volume (which is a quadrilateral with dimensions ΔX and ΔZ) is given by a combination of the temperatures T_N, T_E, T_S, T_W of the four edges (**N**orth, **E**ast, **S**outh, **W**est) of the control volume and the temperature of the preceding iteration cycle T_{P0}:

$$T_P = \frac{a_E T_E + a_W T_W + a_S T_S + a_N T_N + S_C \Delta X \Delta Z + E T_{P0}}{a_E + a_W + a_S + a_N - S_P \Delta X \Delta Z + E} \tag{30}$$

The parameter E is used to enforce the flow directionality (convention) in eq. (30) depending on the difference between the lubricant flow *in* and *out* of the control volume:

$$\begin{aligned} E_1 &= |a_E| + |a_W| + |a_S| + |a_N| - |a_P| \\ E &= E_1 \quad \text{if} \quad E_1 > 0 \\ E &= 0 \quad \text{if} \quad E_1 \le 0 \end{aligned} \tag{31}$$

where

$$\begin{aligned} a_W &= \frac{h_W \Delta X}{2}\left(\rho_W W_W cp_W + \rho_P W_P cp_P\right) \\ a_E &= -\frac{h_E \Delta X}{2}\left(\rho_E W_E cp_E + \rho_P W_P cp_P\right) \\ a_N &= -\frac{h_N \Delta Z}{2}\left(\rho_N U_N cp_N + \rho_P U_P cp_P\right) \\ a_S &= \frac{h_S \Delta Z}{2}\left(\rho_S U_S cp_S + \rho_P U_P cp_P\right) \end{aligned} \tag{32}$$

In the eq. (30), the terms S_C and S_P are obtained from the intensity of the viscous heating S by assuming a linear dependence of the heat source term on the temperature:

$$\begin{aligned} S &= \mu_0 \left[\left(\frac{\partial u}{\partial y}\right)^2 + \left(\frac{\partial w}{\partial y}\right)^2\right] h_P = S_c + S_p T_P \\ S_P &= \frac{S}{\mu_0}\frac{d\mu}{dT} \\ S_C &= S\left(1 - \frac{T_{P0}}{\mu_0}\frac{d\mu}{dT}\right); \end{aligned} \tag{33}$$

where the terms μ_0 and T_{P0} refer to the previous sweep of the iteration for temperature.

In this paper, the temperature of the inlet oil used for the numerical model was maintained at 40°C, which corresponds to the actual operating condition of the bearing.

In conclusion, for a given static load, the following conditions must be satisfied:

- convergence of the pressure distribution in each pad;
- convergence of the temperature distribution in each pad;
- equilibrium of the forces on each pad;
- equilibrium of the forces on the shaft for the given static load.

7. Results and discussion

As previously mentioned, the influence of the load direction to the journal center locus, the dynamic coefficients (in both the absolute and load reference systems), the pressure distribution on each pad and the pad tilt angle are analyzed in this paper using the dynamic model of the complete TPJB and the experimental results.

7.1. Clearance profile and shaft center locus

For the nominal bearing, the numerical journal locus obtained by changing the direction of the static load is a "smoothed pentagon", which can be approximated by a circle with a radius of approximately 30 μm, as shown in Fig. 11 (solid black line with dot markers).

Fig. 11 shows the predicted (black dashed-dotted line) and measured (green solid line) pentagonal clearance profile of the nominal and real TPJBs, respectively. The predicted and measured shaft center locus for the bearing under test and the nominal bearing are plotted inside the measured clearance profile. Twenty positions of the shaft center are measured and correspond to twenty directions of the static load (from −90° to 252°, with steps of 18°). For the test bearing, the journal center loci (the calculated one and the measured one) have irregular shapes.

It should be noted that, although there is a difference between prediction and measurement of the journal center locus, their irregular shapes are similar. This fact is probably due to the flexibility of the system and the thermal expansion of the bearing housing during the experiments. During the experimental tests, while the temperature of the oil input is maintained at approximately 40±1°C

using a heat exchanger and a temperature controller, the temperature of the housing is greater and is approximately equal to 48°C. This causes an expansion of the mechanical components of the bearing.

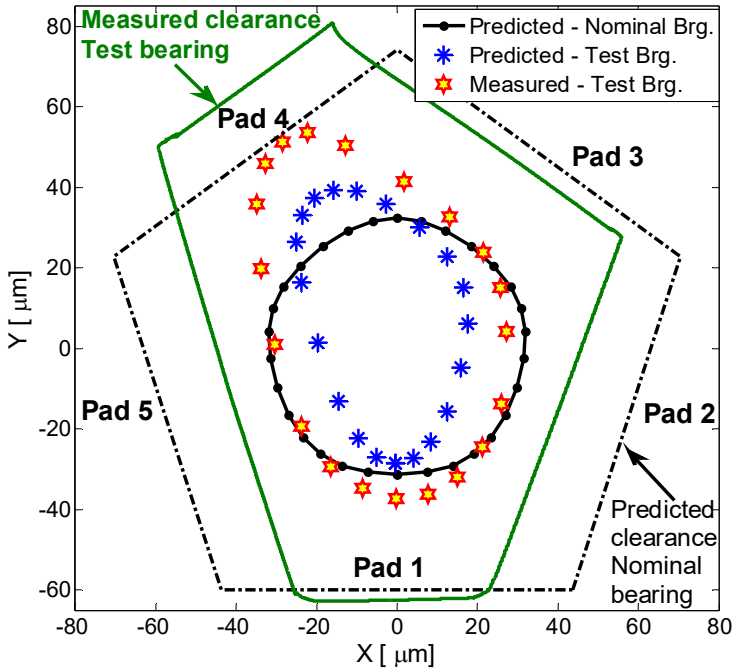

Fig. 11. Shaft center locus of the bearing vs. the load directions

The overall system flexibility include backlashes and stiffness of the system from the pivot to the proximity probe position. These two factors have not been modelled in the mathematical model. The simple thermal model for the oil-film temperature distribution affects the oil-film thickness and pressure distribution. The pivot stiffness considers only the deformation due to the contact between the pad and the bearing housing. The effect of the thermal expansion and system flexibility is a static radial offset in the measurement of the static position of the shaft. Improvement in the model can be obtained by including the additional flexibility of the system in the pivot stiffness given in eq. (23).

It is interesting to observe that the clearance profile of the test bearing, shown in Fig. 11, is greater in the case of pad #4. This effect is likely a consequence of the fact that pad #4 has the

smallest thickness (15.981 mm), so the displacement of the shaft will be greater in the case of pad #4.

7.2. Pressure distributions

The pressure distribution of the oil film is the most fundamental characteristic of journal bearings. The influence of the load directions on the pressure distribution leads to a variation in the static characteristics, dynamic characteristics, and performance of the bearing. The influence of the load directions on the predicted oil-film pressure distributions for the nominal and real bearings is shown in Fig. 12, where only the LOP configurations are considered. It is interesting to note that, when the static load is applied in the vertical direction (–90°) and pad #1 is loaded (see Fig. 4), the pressure on pad #1 is on average less than the pressure on the two adjacent pads, namely, pad #2 and pad #5. The same behavior also occurs when a static load is applied to the middle of pad #4 (126°). Conversely, when the direction of the load is –18° (load on pad #2), 54° (load on pad #3) or 198° (load on pad #5), the oil-film pressure is non-negligible only on pad #2, pad #3, or pad #5, respectively, with a maximum pressure of approximately 4.0 MPa but is negligible on the other pads.

This effect is likely due to the thickness of pads (as listed in Table 2). While it should be noted that the thicknesses of pad #1 (15.994 mm) and pad #4 (15.981 mm) are less than the nominal dimension (16 mm), the thicknesses of other three pads demonstrate an opposite trend. For instance, when a static load of 5 kN is applied in the vertical direction (–90°), the shaft will move toward the middle of pad #1. However, due to smaller thickness in pad #1, the oil-film thickness on average at pad #1 is still greater than the oil-film thickness on pad #2 and pad #5. The theoretical calculations show that the minimum oil-film thickness of pad #1, pad #2, and pad #5 in this case is approximately 35 μm, 31 μm, and 30 μm, respectively. This leads to an average pressure on pad #1 that is less than the pressure on pad #2 and pad #5. It becomes easy to predict that, because the

thickness of pad #5 is the greatest, the pressure on pad #5 will be maximum when the direction of the static load is 198°.

For the nominal bearing, due to the equal dimensions of pads, the oil-film pressure is distributed mainly on the loaded pads with a maximum pressure of approximately 3.5 MPa.

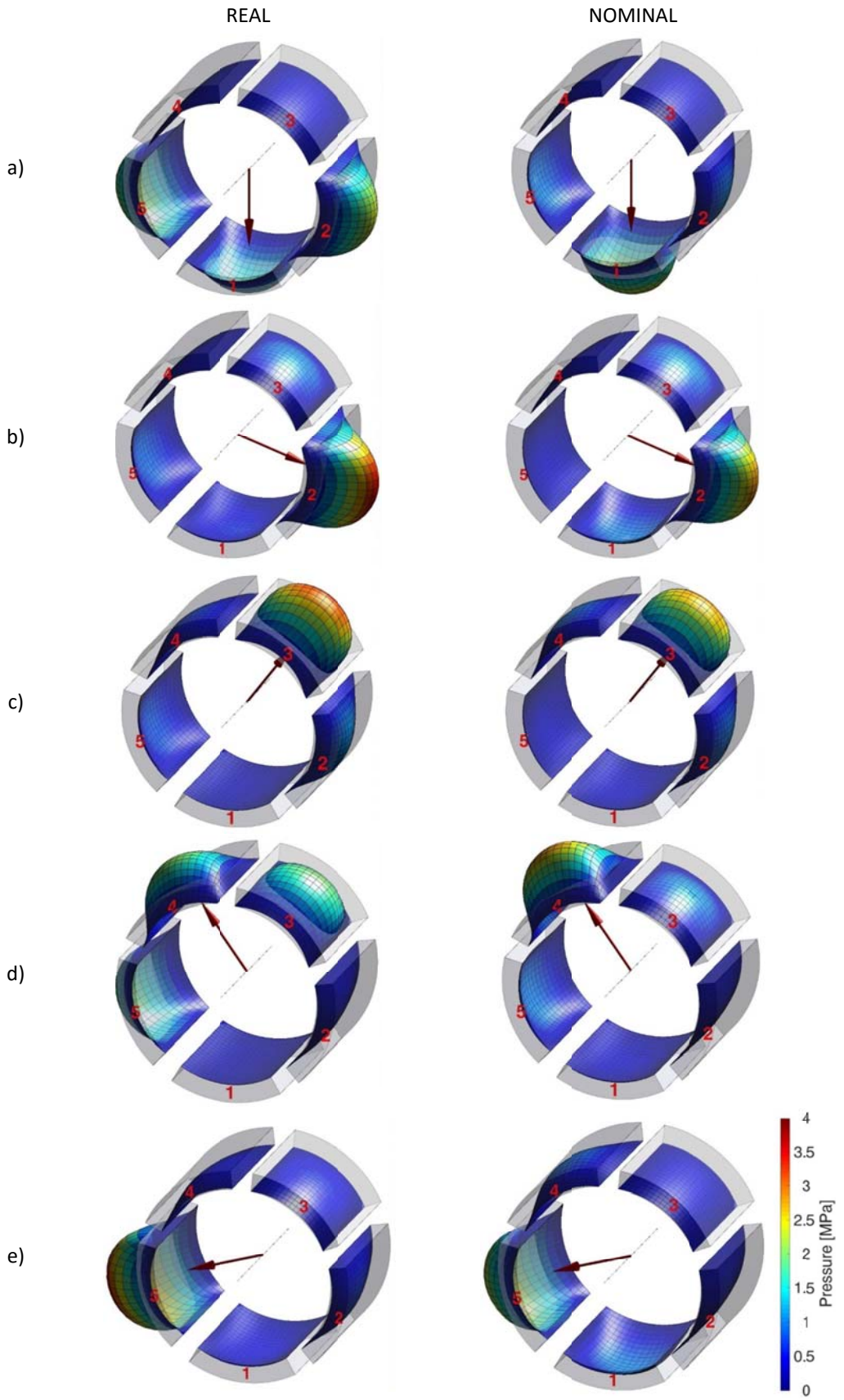

Fig. 12. Pressure distribution of the test bearing (left) and the nominal bearing (right) for LOP configurations

7.3. Pad tilt angle

During operation, the pads rotate about their pivots. It is essential to consider the motion of the pads, which is the pad tilt angle. Fig. 13a shows the predicted pad tilt angle of the nominal five-pad TPJB when the direction of the static load varies. It is easy to observe that the pad tilt angles of all the pads are identical and change periodically with the load direction. The peak-to-peak angle of these pads is approximately 0.05°. To illustrate the impact of an asymmetric geometry, Fig. 13b shows the predicted pad tilt angle of the tested TPJB with changing direction of the static load. It is clear that pads #2, #3, and #5 have greater variation in the pad tilt angle. The peak-to-peak angle of these three pads is approximately 0.05°. Conversely, the tilt angle of pad #1 shows a fairly sinusoidal behavior and the minimum variation in the tilt pad angle of approximately 0.02° peak-to-peak.

a)

b)

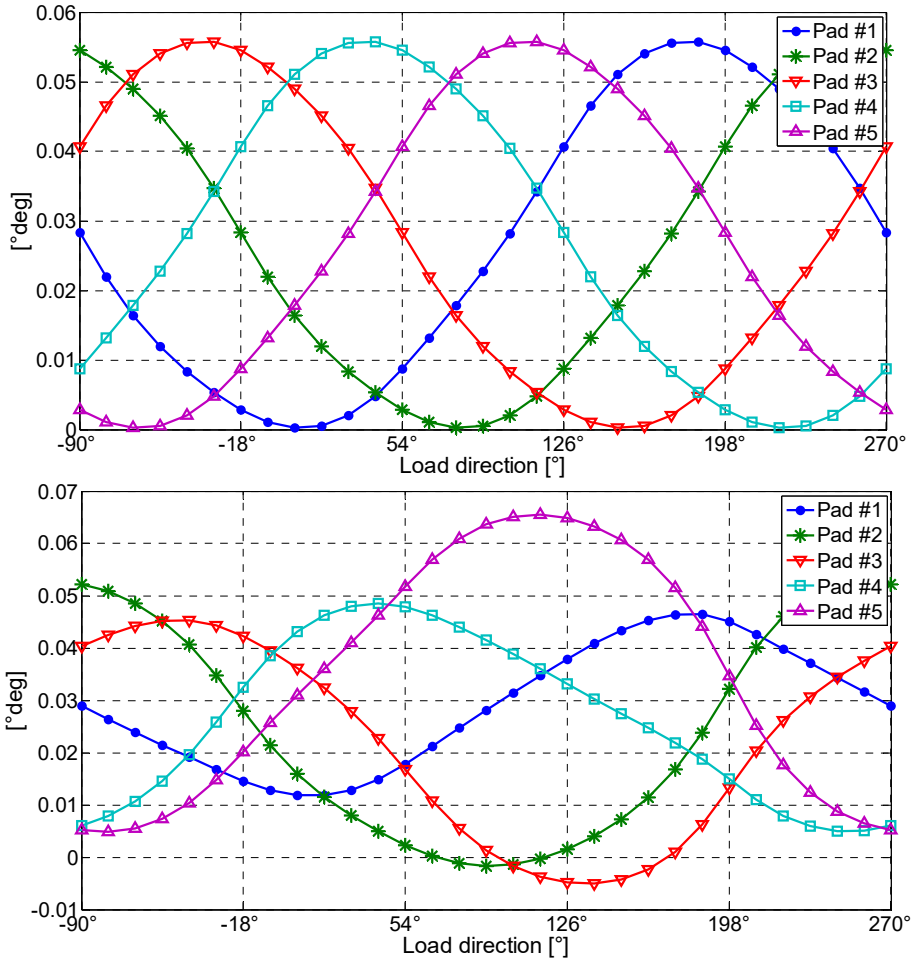

Fig. 13. Pad tilt angle vs. load directions of (a) nominal bearing and (b) test bearing

7.4. Static characteristics

The influence of the load direction on the predicted static characteristics (minimum film thickness $h_{\min}$, flow rate and power loss) is shown in Fig. 14. The results show that the load direction has a strong effect on the minimum oil-film thickness but only has a slight impact on the flow rate and power dissipation. These consequences are consistent with results presented in [15],[17]. It should be noted that the greatest effects on the power loss are attributed to the bearing clearance, rotational speed, bearing length and oil viscosity [17]. Other factors, such as the load direction, have a marginal effect on the power loss.

Moreover, a comparison of these static characteristics is made between the nominal bearing and test bearing. It can be seen that the effect of the asymmetric geometry is significant in terms of flow

rate and power loss. During operation, the flow rate of the test bearing is always smaller compared with the nominal bearing by approximately 10% and vice versa for the power loss. Finally, note that the periodic change in these features does not occur for the bearing under test due to the asymmetric geometry.

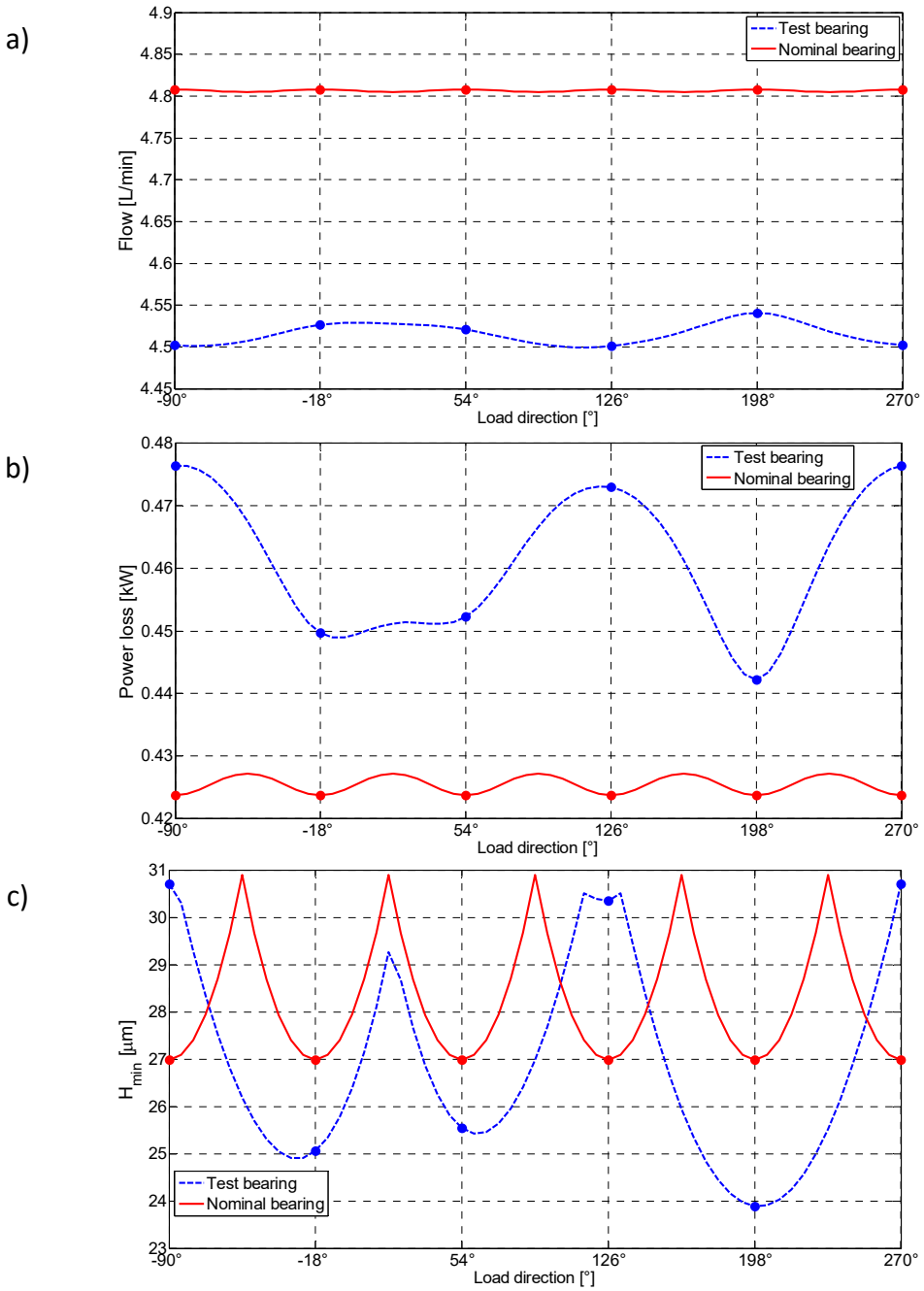

Fig. 14. Influence of the load direction on the static characteristics of TPJBs

7.5. Dynamic coefficients

Two reference systems are introduced here to evaluate the dynamic coefficients, namely, the absolute reference and load reference systems. In the first reference system, a varying load direction is considered, as shown in Fig. 4. In this case, the static load is rotated in a full revolution (360°) in steps of 18°. This means that all five pads will be loaded under a LOP and LBP configuration during the tests.

Fig. 15 shows the influence of the load direction on the experimental and calculated stiffness and damping coefficients of the test bearing. Obviously, the load direction has a strong effect on both of them.

The stiffness coefficients of the test bearing show a general good agreement between the experimental and the calculated values. The differences can be explained, as previously mentioned, by the fact that the measured displacements of the shaft are greater than the calculated ones due to the thermal expansion and flexibility of the housing-pivot system. Consequently, the calculated direct stiffness coefficients are greater than the experimental coefficients. However, this difference is not noteworthy except for the direct stiffness in the horizontal direction (k_{xx}).

The damping coefficients obtained from the experimental tests are rather different from the calculated coefficients; in particular, the calculated direct coefficients (c_{xx} and c_{yy}) are greater than the experimental coefficients. It is also possible to observe in Fig. 15 that the calculated stiffness and damping coefficients of the nominal bearing maintain a certain symmetry as a function of the direction of the load. This is less evident for the test bearing due to the asymmetric geometry.

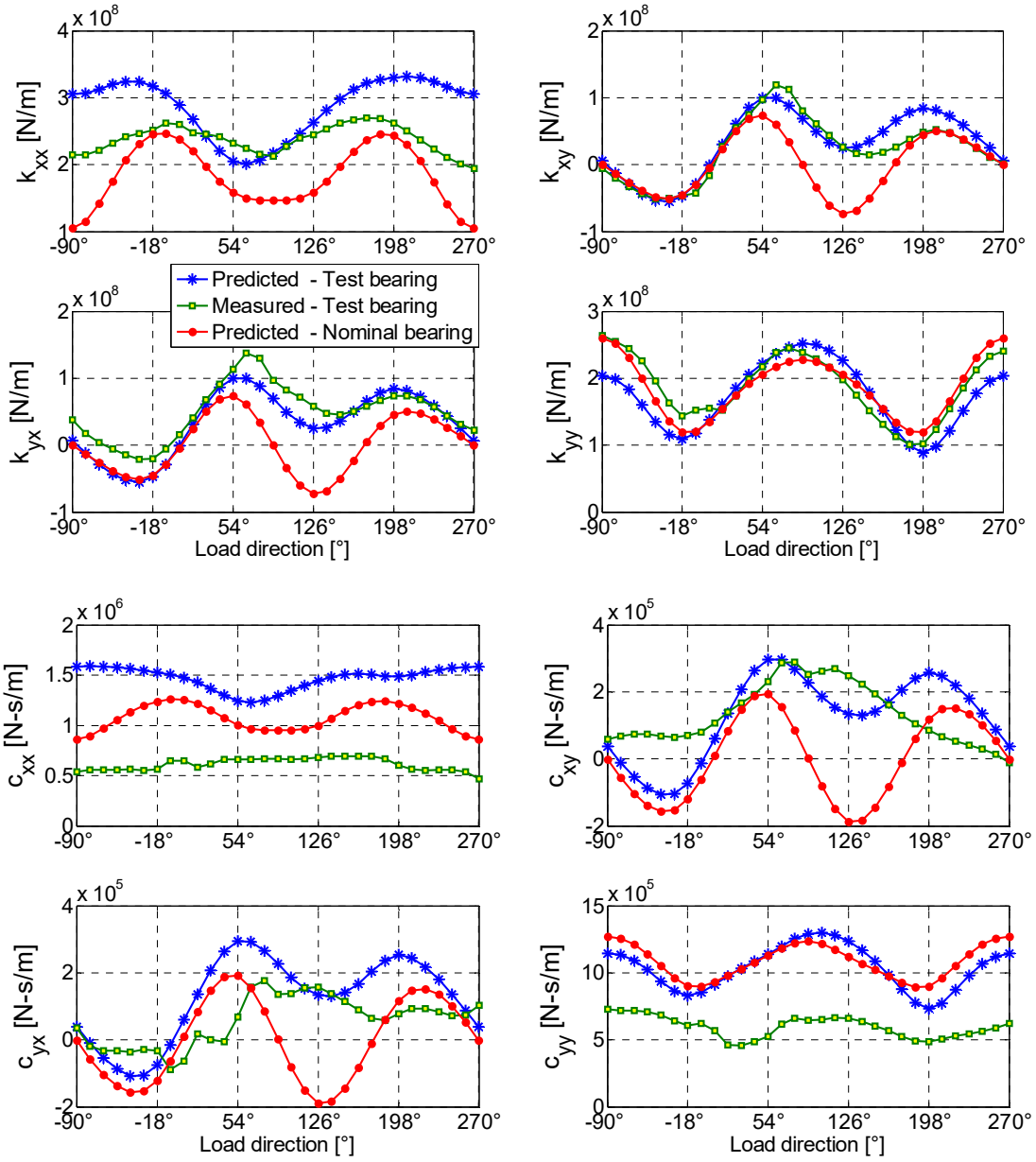

Fig. 15. Dynamic coefficients vs. load directions in the absolute reference system

In the case of the load reference system, the load direction is in a direction opposite to the Y' axis (see Fig. 10b). This corresponds to a rotation of the bearing in which the load is fixed in the vertical direction, as shown in Fig. 16 for LOP configurations.

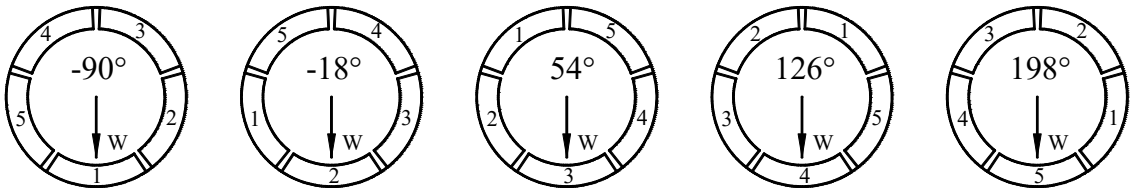

Fig. 16. Varying bearing configuration

The influence of the load direction on the dynamic coefficients in the load reference system is shown in Fig. 17. Whereas the dynamic coefficients of the nominal bearing change periodically with a small fluctuation when the static load rotates, the dynamic coefficients of the bearing under test show large variations.

Similar to the previous varying load configuration, in this case, the measured direct stiffness and damping coefficients were also smaller than the calculated values. Remarkably, among the dynamic coefficients, the cross-coupled stiffness coefficients ($k_{\xi\zeta}$ and $k_{\zeta\xi}$) show the best agreement between the measured and predicted values.

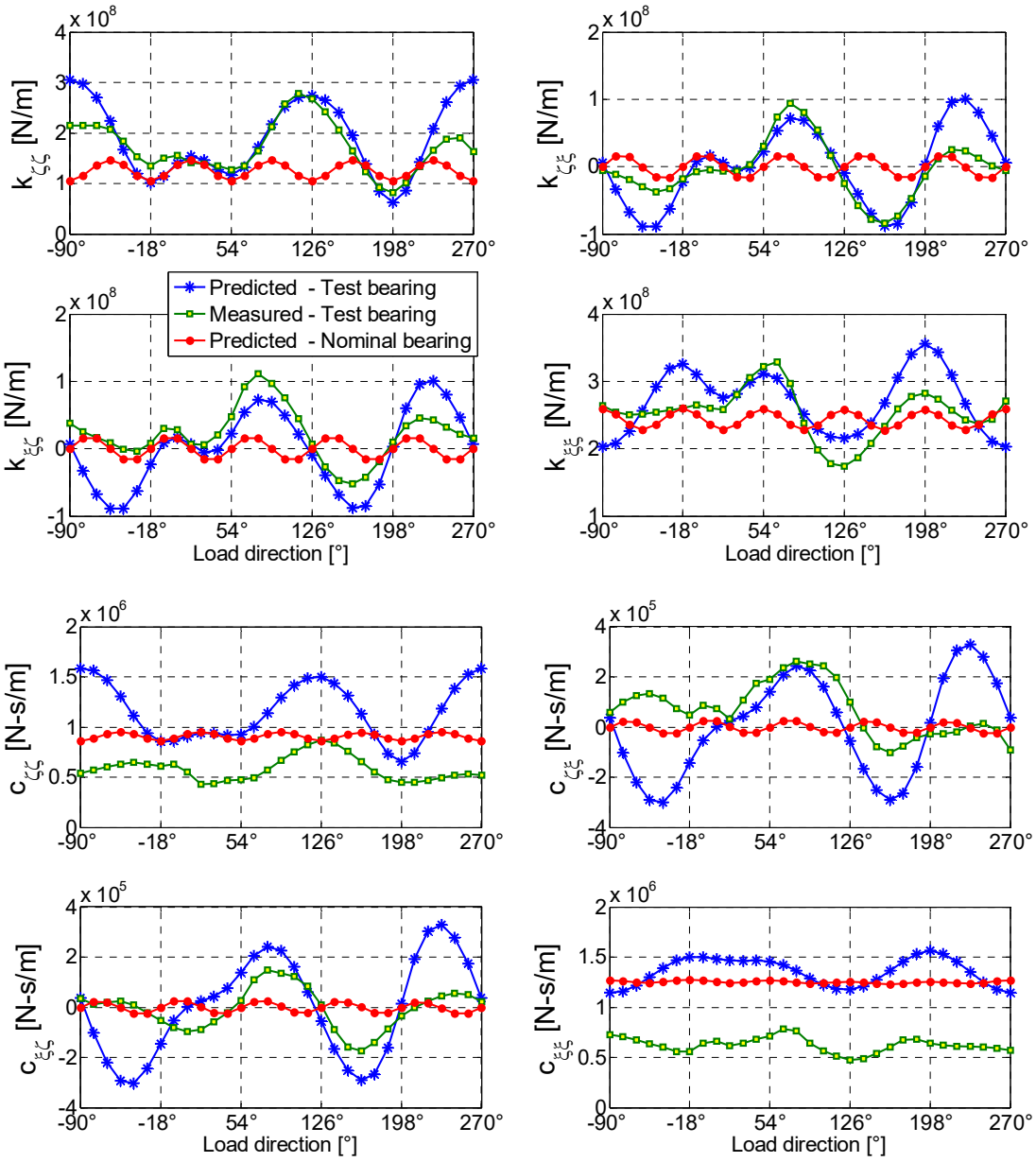

Fig. 17. Dynamic coefficients vs. load directions in the load reference system.

8. Conclusions

In this paper, the effects of load direction on the static and dynamic characteristics of five-pad TPJBs are discussed. The bearing considered in the analysis and in the experimental activity is characterized by a variable assembled clearance for all the pads. This is mainly due to manufacturing and assembling errors in the pads but reflects the actual industrial production. A

comparison is performed with a bearing having nominal (i.e., ideal) geometry. Furthermore, the differences between the experimental and simulated results are also discussed. The procedure for estimating the bearing geometry from the experimental measurements of the non-periodic clearance profile is also described, and a robust estimation technique is introduced for the evaluation of the dynamic coefficients. The following conclusions can be drawn from the numerical and experimental results:

1. The numerical journal locus of nominal bearing obtained by changing the direction of the static load is a "smoothed pentagon", which can be approximated by a circle with a radius of approximately 30 μm. On the contrary, the journal center loci (the prediction as well as measurement) have irregular shapes. This point should be taken into account in the alignment procedures of rotating machines.
2. The load direction has a strong effect on the minimum oil-film thickness but has a slight effect on the oil flow rate and the power dissipation.
3. The influence of the load direction has a stronger effect on the dynamic characteristics of the tilting pad bearing than on the static characteristics.
4. The predicted dynamic coefficients for a non-nominal bearing geometry can be significantly different from those of a nominal geometry. Furthermore, the cross terms are no more negligible if compared to a nominal geometry.
5. In both the load and bearing configurations, the measured direct stiffness and damping coefficients are always smaller than the calculated values. Additionally, among the dynamic coefficients, the cross-coupled stiffness coefficients have the best agreement between measurement and prediction.
6. It is essential to consider the thermal expansion and flexibility of the housing support during the operation of the TPJBs because the static eccentricity measurements may result in errors with respect to both the eccentricity magnitude and the attitude angle

In conclusion, the load direction has a strong effect on the static and dynamic characteristics of tilting pad bearings, especially on the oil-film thickness and the stiffness and damping coefficients. This effect can be amplified or reduced by a non-nominal geometry of the bearing, for which large differences can be detected between the experimental behavior of a real bearing and the predicted behavior obtained using a model of a nominal bearing.

References

[1] Lund JW. Spring and Damping Coefficients for Tilting Pad Journal Bearing. Transactions of the ASLE 1964;7:342-352, doi:10.1080/05698196408972064.

[2] Yan Z, Wang L, Qiao G, Zheng T. An analytical model for complete dynamical coefficients of a tilting-pad journal bearing. Tribol Int 2010; 43:7-15, doi:10.1016/j.triboint.2009.03.010.

[3] Qiuying C, Peiran Y, Yonggang M, Shizhu W. Thermoelastohydrodynamic analysis of the static performance of tilting-pad journal bearings with the Newton–Raphson method. Tribology International 2002;35(4):225-234, doi: 10.1016/S0301-679X(01)00108-6

[4] Dmochowski W, Dadouche A, Fillon M. Numerical study of the sensitivity of tilting-pad journal bearing performance characteristics to manufacturing tolerances: dynamic analysis. Tribology Trans 2008;51(5):573–580, doi: 10.1080/10402000801947709

[5] Strzelecki S. Dynamic characteristics of tilting 5-pads journal bearing with asymmetric support of pads. In: Proceedings of Sixth International Conference on Rotor Dynamics (IFToMM), University of New South Wales, Sydney, Australia 2002; p. 807–814.

[6] Cha M, Isaksson P, Glavatskih S. Influence of pad compliance on nonlinear dynamic characteristics of tilting pad journal bearings. Tribology International 2013;57:46–53, doi:10.1016/j.triboint.2012.07.005

[7] Zhou H, Zhao S, Xu H, Zhu J. An experimental study on oil-film dynamic coefficients. Tribology International 2004;37(3):245–253, doi:10.1016/j.triboint.2003.08.002

[8] Varela AC, Nielsen BB, Santos IF. Steady state characteristics of a tilting pad journal bearing with controllable lubrication: Comparison between theoretical and experimental results. Tribology International 2013;58:85-97, doi:10.1016/j.triboint.2012.10.004

[9] Lihua Y, Huiguang L, Lie Y. Dynamic stiffness and damping coefficients of aerodynamic tilting-pad journal bearings. Tribology International 2007;40(9):1399-1410, doi:10.1016/j.triboint.2007.03.007

[10] Cha M, Glavatskih S. Nonlinear dynamic behaviour of vertical and horizontal rotors in compliant liner tilting pad journal bearings: Some design considerations. Tribology International 2015;82, Part A:142-152. doi:10.1016/j.triboint.2014.10.011

[11] Simmons GF, Varela AC, Santos IF. Dynamic characteristics of polymer faced tilting pad journal bearings. Tribology International 2014;74:20-27, doi:10.1016/j.triboint.2014.02.001

[12] Delgado A, Vannini G, Ertas BM, Drexel M, Naldi L. Identification and Prediction of Force Coefficients in a Five-Pad and Four-Pad Tilting Pad Bearing for Load-on-Pad and Load-Between-Pad Configurations. J. Eng. Gas Turbines Power 2011; 133(9), 092503. doi:10.1115/1.4002864

[13] Solghar AA, Brito FP, Claro JCP, Nassab SAG. An experimental study of the influence of loading direction on the thermohydrodynamic behavior of twin axial grooves journal bearings. Journal of Engineering Tribology 2011;225(5), doi: 10.1177/1350650111401970

[14] Simmons JEL, Dixon SJ. Effect of Load Direction, Preload, Clearance Ratio, and Oil Flow on the Performance of a 200mm Journal Pad Bearing. Transactions of the STLE, Journal of Tribology 1994;37(2):227-236.

[15] Yin M, Chen G, Zhang G. Analysis of Eccentric Load Effect for Tilting Pad Journal Bearing. Transactions of Technology Publications, Applied Mechanics and Materials 2013;364:71-75, doi:10.4028/www.scientific.net/AMM.364.71

[16] Pennacchi P, Vania A, Chatterton S. Nonlinear Effects Caused by Coupling Misalignment in Rotors Equipped with Journal Bearings. Mechanical Systems and Signal Processing 2012;30:306-322, doi:10.1016/j.ymssp.2011.11.020

[17] Jones GJ, Martin FA. Geometry Effects in Tilting-Pad Journal Bearings. Transactions of ASLE 1979;22(3):227-244.

[18] Fillon M, Dmochowski W, and Dadouche A. Sensitivity of Tilting Pad Journal Bearing Performance Characteristics to Manufacturing Tolerances: Steady-State Analysis. Tribology Transactions, 2007, 50, 387-400, doi:10.1080/10402000701429246.

[19] Dmochowski W, Dadouche A, Fillon M. Sensitivity of Tilting Pad Journal Bearing Performance Characteristics to Manufacturing Tolerances: Dynamic Analysis. Tribology Transactions, 2008, 51, 573-580, doi:10.1080/10402000801947709.

[20] Krasker WS. Robust regression. S. Kotz, N.L. Johnson, C.B. Read, N. Balakrishnan, B. Vidakovic (Eds.), Encyclopedia of Statistical Sciences, 8, Wiley, New York, 1983, 166–169.

[21] Bickel P. Robust estimation. S. Kotz, N.L. Johnson, C.B. Read, N. Balakrishnan, B. Vidakovic (Eds.), Encyclopedia of Statistical Sciences, 8, Wiley, New York, 983, 157–163.

[22] Huber PJ. Robust Statistics, Wiley, New York, 1981.

[23] Hori Y. Hydrodynamic Lubrication. 1st ed. Verlag Tokyo: Springer; 2006.

[24] Chatterton S, Pennacchi P, Dang PV, Vania A. A Test Rig for Evaluating Tilting–Pad Journal Bearing Characteristics. In: Proceedings of 9th International Conference on Rotor Dynamics (IFToMM); 2014 September 22-25; Milan, Italy; 21: 921-930, doi: 10.1007/978-3-319-06590-8_75

[25] Chatterton S, Pennacchi P, Dang PV, Vania A. Identification Dynamic Force Coefficients of a Five-Pad Tilting-Pad Journal Bearing. In: Proceedings of 9th International Conference on Rotor Dynamics (IFToMM); 2014 September 22-25; Milan, Italy; 21: 931-941, doi: 10.1007/978-3-319-06590-8_76

[26] Dang PV, Chatterton S, Pennacchi P, Vania A, Cangioli F. Behavior of a Tilting–Pad Journal Bearing With Different Load Directions, ASME Paper No. DETC2015-46598, 2015; 8. doi:10.1115/DETC2015-46598

[27] Dang PV, Chatterton S, Pennacchi P, Vania A, Cangioli F. An Experimental Study of Nonlinear Oil-Film Forces in a Tilting-Pad Journal Bearing, ASME Paper No. DETC2015-46601, 2015; 8. doi:10.1115/DETC2015-46601

[28] Pennacchi P. Robust estimate of excitations in mechanical systems using M-estimators-theoretical background and numerical applications, Journal of Sound and Vibration, 2008; 310(4-5): 923–946. doi:10.1016/j.jsv.2007.08.007

[29] Ricci R, Chatterton S, Pennacchi P. Robust estimation of excitation in mechanical systems under model uncertainties. Journal of Sound and Vibration, 2013; 332(2):264–281. doi:10.1016/j.jsv.2012.08.022

[30] Street JO, Carrol RJ, Ruppert D. A note on computing robust regression estimates via iteratively reweighted least squares. Journal of the American Statistical Association, 1988;42(2):152–154. doi:10.2307/2684491

[31] Rouvas C, Childs D. A Parameter Identification Method for the Rotordynamic Coefficients of a High Renoylds Number Hydrostatic Bearing. J. Vib. Acoust 1993;115(3):264-270. doi: 10.1115/1.2930343

[32] Wilkes JC, Childs DW. Tilting Pad Journal Bearing - A Discussion on Stability Calculation, Frequency Dependence, and Pad and Pivot. J. Eng. Gas Turbines Power 2012;134(12), 122508. doi: 10.1115/1.4007369

[33] Dang PV, Chatterton S, Pennacchi P, Vania A, Cangioli F. Eccentricity Measurements on a Five-pad Tilting Pad Journal Bearing. In: Proceedings of the 14th IFToMM World Congress, Taipei, Taiwan, October 25-30,2015. doi: 10.6567/IFToMM.14TH.WC.OS14.020

[34] Dang PV, Chatterton S, Pennacchi P, Vania A, Cangioli F. Investigation of Load Direction on a Five-Pad Tilting Pad Journal Bearing with Variable Clearance. In: Proceedings of the 14th IFToMM World Congress, Taipei, Taiwan, October 25-30,2015. doi: 10.6567/IFToMM.14TH.WC.OS14.021

[35] Kirk RG, and Reedy SW. Evaluation of Pivot Stiffness for Typical Tilting-Pad Journal Bearing Designs. J. Vib., Acoustics, Stress, and Reliability in Design, 1988; 110:165-171.

[36] Stachowiak GW, Batchelor AW. - Engineering Tribology, Butterworth-Heinemann, 2011.